Star Formation from Turbulent Fragmentation

Ralf Klessen

Sterrewacht Leiden, Postbus 9513, 2300-RA Leiden, The Netherlands

Abstract. Star formation is intimately linked to the dynamical evolution of molecular clouds. Turbulent fragmentation determines where and when protostellar cores form, and how they contract and grow in mass via accretion from the surrounding cloud material. Efficiency, spatial distribution and timescale of star formation in turbulent clouds are estimated by comparing numerical models of self-gravitating isothermal gas where turbulence is assumed to have decayed or is driven at supersonic speed on various wavelengths. Turbulence that is not continuously replenished or that is driven on large scales leads to a rapid formation of stars in a clustered mode, whereas interstellar turbulence that carries most energy on small scales results in isolated star formation with low efficiency. Protostellar accretion rates strongly vary in time and peak at a few $10^{-5}\,\mathrm{M}_\odot\,\mathrm{yr}^{-1}$. The clump mass spectrum for models of pure hydrodynamic turbulence is steeper than the observed one, but becomes comparable when including gravity. The mass spectrum of dense cores, on the other hand, is log-normal for decaying and large-wavelength turbulence, similar to the IMF, but is to flat in the case of small-scale turbulence.

1. Introduction

Understanding the processes that lead to the formation of stars is one of the fundamental challenges in astronomy. Stars are born in turbulent interstellar clouds of molecular hydrogen. The location and the mass growth of young stars are hereby intimately coupled to the dynamical cloud environment. Stars form by gravitational collapse of shock compressed density fluctuation generated from the supersonic turbulence ubiquitously observed in molecular cloud (e.g. Padoan 1995, Klessen, Heitsch, & Mac Low 2000). Once a gas clump becomes gravitationally unstable, collapse progresses in the center until a protostellar object forms which continues to grow in mass via accretion from the infalling envelope (see Wuchterl, this volume). Also, stars hardly ever form in isolation. Instead they come in small aggregates or larger clusters (Lada 1992, Mizuno et al. 1995, Testi, Palla, & Natta 1998), where the interaction of protostellar cores and their competition for mass from their surrounding are important processes shaping the distribution of the final star properties.

Star formation can thus be seen as a two-phase process: First, *turbulent fragmentation* leads to transient clumpy molecular cloud structure, with some of the density fluctuation exceeding the critical mass and density for gravitational contraction. This sets the stage for the second phase of star formation, the

collapse of individual protostellar clumps building up central protostars. In the following, the words gas clump and shock-generated density fluctuation are used synonymously. Cores are defined as the high-density central regions of collapsing clumps where protostars build up. I focus on the first phase of star formation and demonstrate how the turbulent interstellar velocity field influences the properties of forming stellar aggregates and clusters. Using numerical simulations (§2) of decayed and driven supersonic turbulence in self-gravitating isothermal gas as templates for molecular cloud dynamics, I discuss the spatial distribution and timescale (§3) of star formation, the resulting protostellar accretion rates (§4), and the expected mass spectra for gas clumps and protostellar cores (§5).

2.   Numerical Method and Driven Turbulence

To adequately describe turbulent fragmentation and the formation of protostellar cores, it is necessary to resolve the collapse of shock compressed regions over several orders of magnitude in density. Due to the stochastic nature of supersonic turbulence, it is not known in advance where and when local collapse occurs. Hence, SPH (*smoothed particle hydrodynamics*) is used to solve the equations of hydrodynamics. It is a Lagrangian method, where the fluid is represented by an ensemble of particles and flow quantities are obtained by averaging over an appropriate subset of the SPH particles (Benz 1990). High density contrasts are resolved by simply increasing the particle concentration where needed. SPH can also be combined with the special-purpose hardware device GRAPE (Sugimoto et al. 1990, Ebisuzaki et al. 1993; also Steinmetz 1996) permitting calculations at supercomputer level on a normal workstation. The simulations presented here concentrate on subregions within a much larger cloud, therefore periodic boundary conditions are adopted (Klessen 1997). The high-density cores of collapsing gas clumps are substituted by 'sink' particles (Bate, Bonnell & Price 1995) while keeping track of mass and momentum.

The large observed linewidths in molecular clouds imply the presence of supersonic velocity fields that carry enough energy to counterbalance gravity on global scales (Williams, Blitz, & McKee 2000). However, it is known that turbulent energy dissipates rapidly, roughly on the free-fall timescale (Mac Low et al. 1998, Stone, Ostriker, & Gammie 1998, Padoan & Nordlund 1999). Unlike previously thought, this is independent of the presence of magnetic fields. For the current models the fields are therefore assumed to be dynamically unimportant and not included. To prevent or considerably postpone global collapse, turbulence is required to be continuously replenished. This is achieved by applying a Gaussian driving scheme, that inserts kinetic energy in a specified range of wavenumbers, $1 \leq k \leq 2$, $3 \leq k \leq 4$, and $7 \leq k \leq 8$, corresponding to sources that act on large, intermediate, and small scales, respectively (Klessen et al. 2000, models $\mathcal{B}1h$, $\mathcal{B}2h$, and $\mathcal{B}3h$). The energy input at each timestep is adjusted to reach a constant level of total kinetic energy, sufficient to stabilize the cloud as a whole. For comparison, I also include one molecular cloud model where turbulence already is decayed and leaves behind a Gaussian density field which begins to contract on all scales (Klessen & Burkert 2000, model $\mathcal{I}$).

The models presented here are computed in normalized units. If scaled to mean densities of $n(\mathrm{H}_2) = 10^5 \, \mathrm{cm}^{-3}$, a value typical for star-forming molecu-

lar cloud regions (e.g. in ρ-Ophiuchus, see Motte, André, & Neri 1998) and a temperature of $11.4\,\mathrm{K}$ (i.e. a sound speed $c_{\mathrm{s}} = 0.2\,\mathrm{km/s}$), then the total mass contained in the computed volume is $130\,\mathrm{M_\odot}$ and the size of the cube is $0.29\,\mathrm{pc}$. It contains 64 thermal Jeans masses.

3. Spatial Distribution and Timescale of Star Formation

Stars form from turbulent fragmentation of molecular cloud material. Super-sonic turbulence that is strong enough to counterbalance gravity on global scales will usually provoke *local* collapse. Turbulence establishes a complex network of interacting shocks, where converging shockfronts generate clumps of high density. This density enhancement can be large enough for the fluctuations to become gravitationally unstable and collapse, when the local Jeans length becomes smaller than the size of the fluctuation. However, the fluctuations in turbulent velocity fields are highly transient. The random flow that creates local density enhancements can disperse them again. For local collapse to actually result in the formation of stars, locally Jeans-unstable shock-generated density fluctuations must collapse to sufficiently high densities on time scales shorter than the typical time interval between two successive shock passages. Only then are they able to 'decouple' from the ambient flow pattern and survive subsequent shock interactions. The shorter the time between shock passages, the less likely these fluctuations are to survive. Hence, the efficiency of protostellar core formation and the rate of continuing accretion onto collapsed cores depend strongly on the wavelength and strength of the driving source (Klessen et al. 2000).

The velocity field of long-wavelength turbulence is dominated by large-scale shocks which are very efficient in sweeping up molecular cloud material, thus creating massive coherent structures. When a coherent region reaches the critical density for gravitational collapse its mass typically exceeds the local Jeans limit by far. Inside the shock compressed region, the velocity dispersion is much smaller than in the ambient turbulent flow and the situation is similar to localized turbulent decay. Quickly a cluster of protostellar cores builds up. Both, decaying and large-scale turbulence therefore lead to a *clustered* mode of star formation. The efficiency of turbulent fragmentation is reduced if the driving wavelength decreases. When energy is carried mainly on small spatial scales, the network of interacting shocks is very tightly knit, and protostellar cores form independently of each other at random locations throughout the cloud and at random times. Individual shock generated clumps have lower mass and the time interval between two shock passages through the same point in space is small. Hence, collapsing cores are easily destroyed again and star formation is inefficient. This scenario corresponds to the *isolated* mode of star formation. It needs to be pointed out that there is no fundamental dichotomy between the two modes of star formation, they rather define the extreme ends in the continuous spectrum of the properties of turbulent molecular cloud fragmentation.

This is visualized in Fig. 1. It compares the models of decayed, large-wavelength ($k = 1\ldots2$), intermediate ($k = 3\ldots4$), and small-scale turbulence ($k = 7\ldots8$). The density structure of the systems is depicted at $t = 0$, which means for the model of decayed turbulence that the initial Gaussian density field is visible. For the driven models, $t = 0$ corresponds to the phase of fully devel-
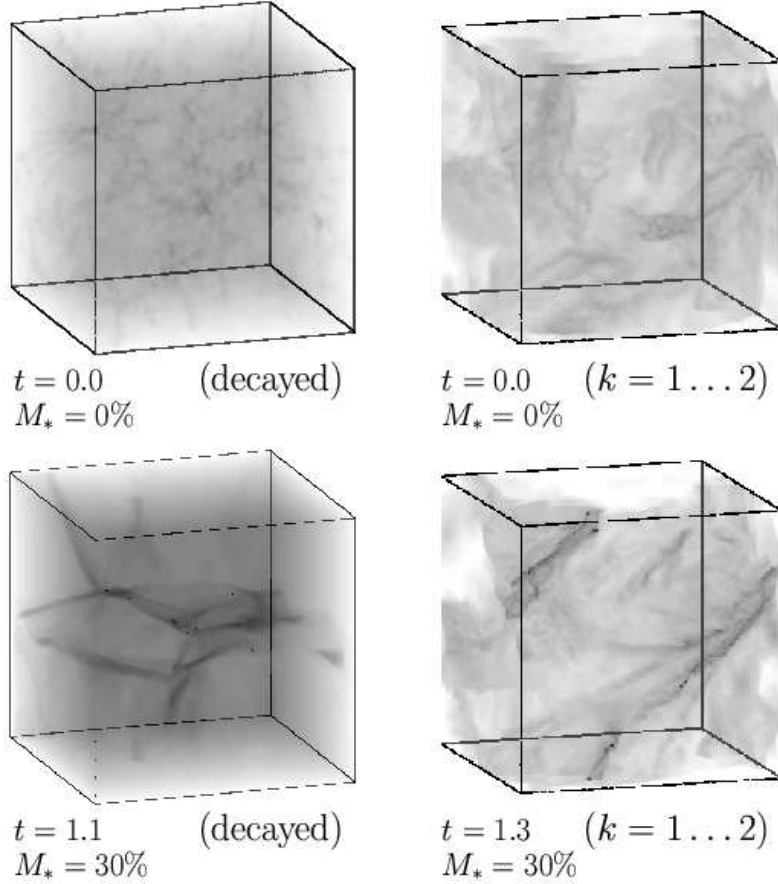
Figure 1.   Comparison of the gas distribution in the models: decayed turbulence (left column) and large-scale turbulence (right column). The upper panel depicts the initial stage when gravity is 'turned on', the lower panel shows system after the first cores have formed and accumulated roughly 30% of the total mass.

oped turbulence just before gravity is 'switched on'. The lower panel describes the four models after the first protostellar cores have formed via turbulent fragmentation and have accreted 30% of the total mass. Time is measured in units of the global free-fall timescale $\tau_{\mathrm{ff}} = (3\pi/32G)^{-1/2} \langle\rho\rangle^{-1/2}$, with $\langle\rho\rangle$ being the mean density. Dark dots indicate the location of dense collapsed core. As for decayed turbulence all spatial modes are unstable, the system quickly evolves into a network of intersecting filaments, where protostellar cores predominantly form. Similarly, also large-scale turbulence builds up a network of filaments, however, this time the large coherent structures are not caused by gravity, but instead are due to shock compression. Once gravity is included, it quickly dominates the evolution inside the dense regions and again a cluster of protostellar cores builds up. In the case of intermediate-wavelength turbulence, cores form in small aggregates, whereas small-scale turbulence leads to local collapse of individual objects randomly dispersed throughout the volume. Note the different times

$t = 0.0 \quad (k = 3 \ldots 4)$
$M_* = 0\%$

$t = 0.0 \quad (k = 7 \ldots 8)$
$M_* = 0\%$

$t = 1.8 \quad (k = 3 \ldots 4)$
$M_* = 30\%$

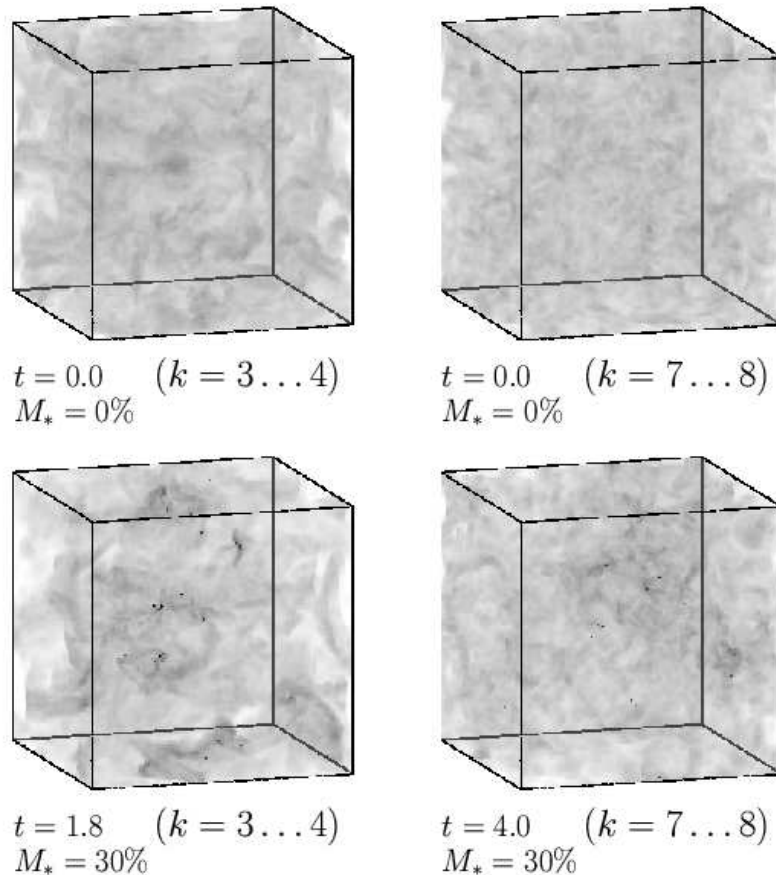$t = 4.0 \quad (k = 7 \ldots 8)$
$M_* = 30\%$

Figure 1. — continued: Comparison of the gas distribution in the models: intermediate-wavelength turbulence (left column) and small-wavelength turbulence (right column).

needed for 30% of the mass to be accumulated in dense cores. For small-scale turbulence star formation progresses slowest, but the process speeds up with increasing driving wavelength. The collapse rates for large-scale turbulence and locally decayed turbulence are comparable. This is further exemplified in Fig. 2, which shows the mass accretion history of individual protostellar cores for the three turbulent models, together with the distribution of core formation times. Star formation efficiency is high in the long-wavelength model, all cores form within two free-fall times, whereas in the short-wavelength model the efficiency is low and core formation continues for over $15\,\tau_{\mathrm{ff}}$ (when the simulation was stopped).

4. Protostellar Accretion Rates

In a dynamical cloud environment the mass accretion rates onto collapsing protostellar cores are strongly *time variable*. This is already visible in Fig. 2, and
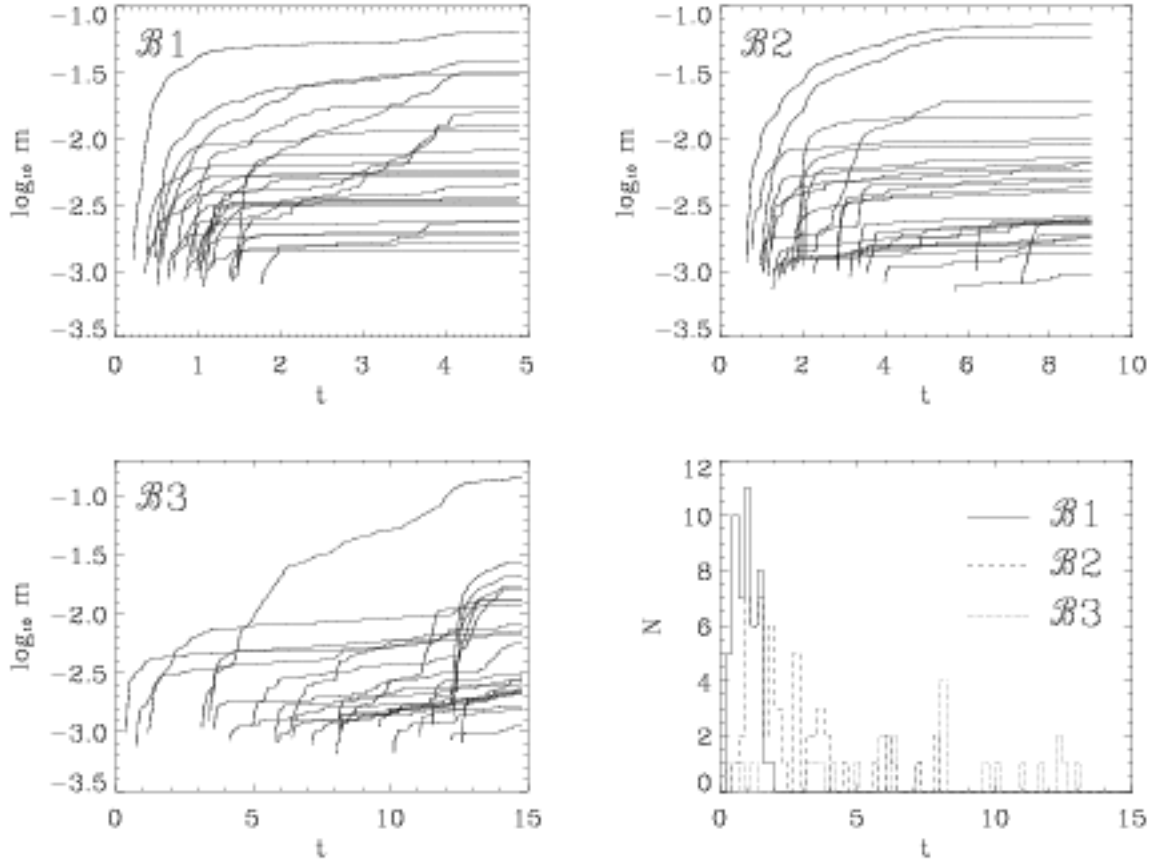
Figure 2. Mass growth history of protostellar cores (only every second core is depicted): long-wavelength ($\mathcal{B}1h$), intermediate- ($\mathcal{B}2h$), and small-scale turbulence ($\mathcal{B}3h$). The lower left plot shows the distribution of the formation times of the cores. Time is again given in units of τ_{ff} and masses are scaled to the total mass in the system.

is quantified in more detail in Fig. 3. It shows dM/dt as function of mass M and time t in each model for the protostellar core which final mass is nearest to $1\,\mathrm{M}_\odot$. To obtain mass M and time t in physical units, the models are scaled to a temperature $T = 11.4\,\mathrm{K}$ and a mean density $n(\mathrm{H}_2) = 10^5\,\mathrm{cm}^{-3}$. The accretion rate dM/dt is insensitive to the adopted scaling, as M and t behave analogously, e.g. if $n(\mathrm{H}_2)$ is decreased by 100, then mass and timescale go up by a factor 10. The current models yield peak accretion rates of a few $10^{-5}\,\mathrm{M}\,\mathrm{yr}^{-1}$ during the initial phase of protostellar collapse. For undisturbed cores, the accretion rates then rapidly decline in the subsequent evolution. This decrease is expected for dynamical collapse and is suggested by observations (e.g. Hendriksen, André, & Bontemps 1997). In a dynamical cloud environment, however, additional peaks of strong accretion are likely to occur. Their duration and strength are highly probabilistic. In the case of large-scale collapse, variations of dM/dt mostly result from clump mergers which modify the immediate surrounding of the accreting cores. In turbulent clouds, most secondary accretion peaks are due to additional shock interaction. Again, gas is compressed in the vicinity the protostar and the accretion rate increases.

The environmental variation of the accretion rates will impact the observational properties of forming protostars. As the accretion luminosity is proportional to the accretion rate, considerable deviations are expected between the
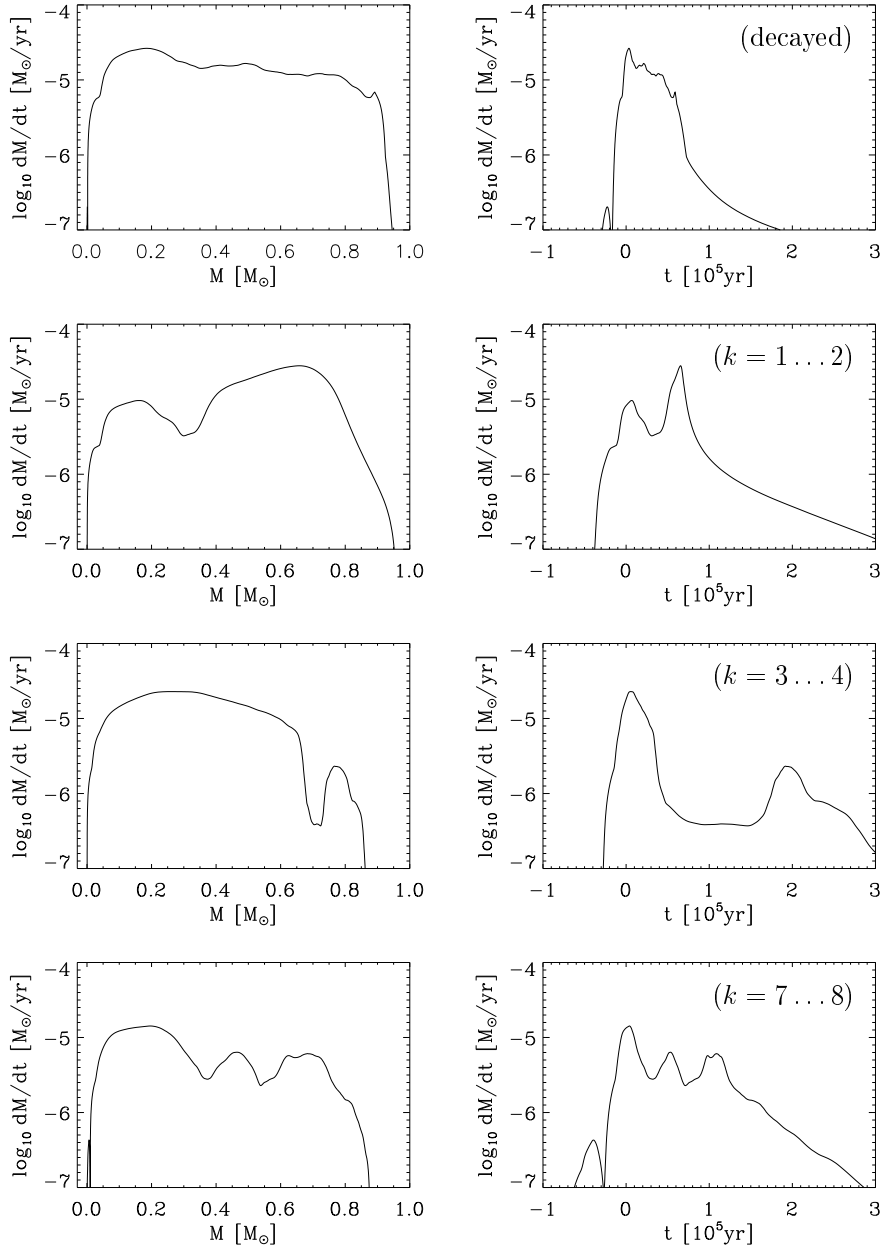
Figure 3.   Accretion rates as function of mass and time for the protostellar cores with final mass closest to $1\,M_\odot$. The four models are scaled to a temperature $T = 11.4\,K$ and a mean density $n(H_2) = 10^5\,cm^{-3}$. Note, that the rate dM/dt is independent of the adopted scaling, mass M and time t change synchronous. The depicted time interval is chosen such that the formation of the protostellar core ('sink' particle) is at $t = 0$. Values of dM/dt for $t < 0$ are due to turbulent compression.

pre-main sequence evolutionary tracks of protostars of the same mass and age but different mass growth histories (see also Wuchterl, this volume).

5.   Mass Spectra of Clumps and Protostellar Cores

The dominant parameter determining stellar evolution is the mass. It is therefore important to investigate the relation between the masses of molecular clumps, protostellar cores and the resulting stars. Figure 4 plots for the four models the mass distribution of all gas clumps, of the subset of Jeans-critical clumps, and of collapsed cores. Three different evolutionary phases are shown, initially just when gravity is 'switched on', and then after turbulent fragmentation has lead to significant protostellar core formation when $M_* \approx 30\%$ and $M_* \approx 60\%$, respectively. In the late stages the gravitational potential is dominated by the dense cores. Clumps are defined based on a method proposed by Williams, De Geus, & Blitz (1994), which has been adapted to the SPH algorithm and makes use of all three spatial coordinates (see Appendix 1 in Klessen & Burkert 2000).

In the initial, completely pre-stellar phase the clump mass spectrum is very steep (about Salpeter slope or less) at the high-mass end and gets shallower below $M \approx 0.4 \langle M_J \rangle$ with slope -1.5, when using a power-law fit to dN/dM. The spectrum strongly declines beyond the SPH resolution limit. Altogether, individual clumps are rarely more massive than one or two $\langle M_J \rangle$. This distribution is similar to what Motte et al. (1998) find for pre-stellar condensations in ρ-Ophiuchus. Recall that for densities of $n(H_2) = 10^5 \, \mathrm{cm}^{-3}$ and temperatures $T = 11.4 \, \mathrm{K}$, the mean Jeans mass in the system is $\langle M_J \rangle \approx 1 \, \mathrm{M}_\odot$.

Gravity strongly modifies the distribution of clump masses during the later evolution. As gas clumps merge and grow bigger, their mass spectrum becomes flatter and extends towards larger masses. Consequently, the number of clumps that exceed the Jeans limit grows, and local collapse sets in leading to the formation of dense condensations. This is most evident in the model of decayed turbulence, where the velocity field is entirely determined by gravitational contraction on all scales. The clump mass spectrum in intermediate phases of the evolution (i.e. when protostellar cores are forming, but the overall gravitational potential is still dominated by non-accreted gas) exhibits a slope -1.5 similar to the observed one. When the velocity field is dominated by strong (driven) turbulence, the effect of gravity on the clump mass spectrum is much weaker. It remains steep, close to or even below the Salpeter value. This is most clearly seen for small-wavelength turbulence. Here, the short interval between shock passages prohibits efficient merging and the build up of a large number of massive clumps. Only few fluctuations become Jeans unstable and collapse to form protostars. These form independent of each other at random locations and times and typically do not interact. Increasing the driving wavelength leads to more coherent and rapid star formation. It also results in a larger number of protostars, which is maximum in the case of pure gravitational contraction (i.e. decayed turbulence).

Long-wavelength turbulence or turbulent decay leads to a core mass spectrum that is well approximated by a *log-normal*. It roughly peaks at the *average thermal Jeans mass* $\langle M_J \rangle$ of the system and is comparable in width with the
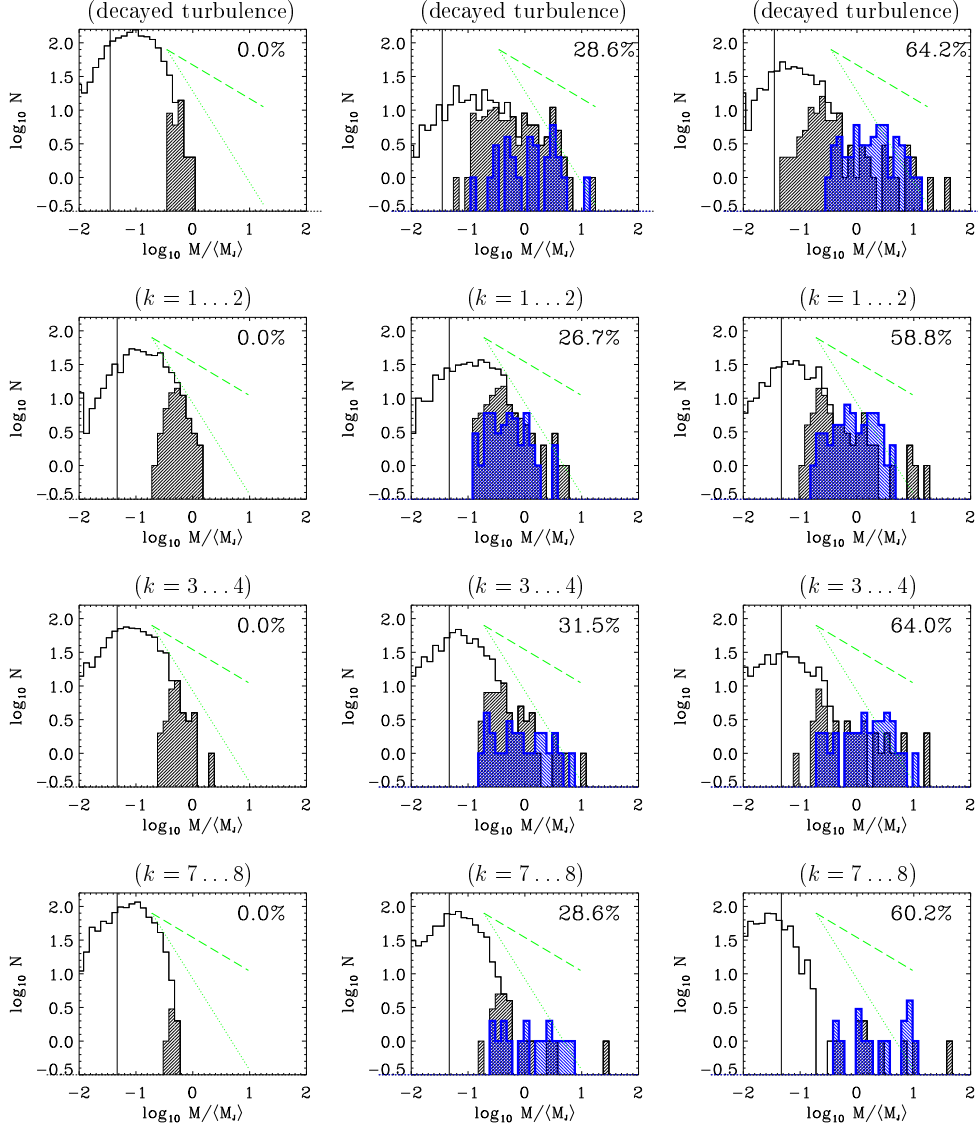
Figure 4. Mass spectra of dense collapsed cores (hatched thick-lined histograms), of gas clumps (thin lines), and of the subset of Jeans unstable clumps (thin lines, hatched distribution). Masses are binned logarithmically and normalized to the average Jeans mass $\langle M_{\rm J} \rangle$. The left column gives the initial state of the system, just when gravity is 'switched on', the middle column shows the mass spectra when roughly 30% of the mass is in dense cores, and the right column when this fraction is about 60%. For comparison with power-law spectra ($dN/dM \propto M^\nu$), the typical slope $\nu = -1.5$ of the observed clump mass distribution, and the Salpeter slope $\nu = -2.33$ for the IMF, are indicated by the long dashed and by the dotted lines in each plot. The vertical line shows the SPH resolution limit.

observed IMF (Klessen & Burkert 2000). The log-normal shape of the mass distribution may be explained by invoking the central limit theorem (e.g. Zinnecker 1984), as protostellar cores form and evolve through a sequence of highly stochastic events (resulting from supersonic turbulence and/or competitive accretion). To find the mass peak at $\langle M_{\mathrm{J}} \rangle$ may be somewhat surprising given the fact that the local Jeans mass strongly varies between different clumps. In a statistical sense the system retains knowledge of its mean properties. The total width of the core distribution is about two orders of magnitude in mass and is approximately the same for all four models. However, the spectrum for intermediate and short-wavelength turbulence, i.e. for isolated core formation, is too flat (or equivalently too wide) to be comparable to the observed IMF. This is in agreement with the hypothesis that most stars form in aggregates or clusters.

References

Benz, W., 1990, in The Numerical Modeling of Nonlinear Stellar Pulsations, ed. J. R. Buchler (Dordrecht: Kluwer), 269

Bate, M.R., Bonnell, I.A, Price, N.M. 1995, MNRAS, 277, 362

Ebisuzaki, T., Makino, J., Fukushige, T., Taiji, M., Sugimoto, D., Ito, T., Okumura, S. K., 1993, PASJ, 45, 269

Henriksen, R., André, P., Bontemps, S., 1997, A&A, 323, 549

Klessen, R. S., 1997, MNRAS, 292, 11

Klessen, R. S., Burkert, A., 2000, ApJS, 128, 287

Klessen, R. S., Heitsch, F., Mac Low, M.-M., 2000, ApJ, 535, 887

Lada, E., 1992, ApJ, 393, L25

Mac Low, M.-M., Klessen, R. S., Burkert, A., Smith, M. D., 1998, Phys.Rev.Lett, 80, 2754

Mizuno, A., Onishi, T., Yonekura, Y., Nagahama, T., Ogawa, H., Fukui, Y. 1995, ApJ, 445, L161

Motte, F., André, P., Neri, R., 1998, A&A, 336, 150

Padoan, P., 1995, MNRAS, 277, 337

Padoan, P., Nordlund, Å., 1999, ApJ, 526, 279

Steinmetz, M., 1996, MNRAS, 278, 1005

Stone, J. M., Ostriker, E. C., Gammie, C. F., 1998, ApJ, 508, L99

Sugimoto, D., Chikada, Y., Makino, J., Ito, T., Ebisuzaki, T., Umemura, M., 1990, Nature, 345, 33

Williams, J. P., Blitz, L., McKee, C. F., 2000, in Protostars and Planets IV, eds. V. Mannings, A. Boss, & S. Russell, in press (astro-ph/9902246)

Williams, J. P., De Geus, E., Blitz, L., 1994, ApJ, 428, 693

Testi, L., Palla, F., Natta, A., 1998, A&A, 342, 515

Zinnecker, H., 1984, MNRAS, 210, 43